01 Oct 1995

Coherent Excitation of the Singlet-triplet Mixed 1s4f State of Helium

Jingbo Wang

J. F. Williams

Andris T. Stelbovics

John E. Furst

et. al. For a complete list of authors, see https://scholarsmine.mst.edu/phys_facwork/1543

Recommended Citation

J. Wang et al., "Coherent Excitation of the Singlet-triplet Mixed 1s4f State of Helium," *Physical Review A - Atomic, Molecular, and Optical Physics*, vol. 52, no. 4, pp. 2885-2900, American Physical Society (APS), Oct 1995.

The definitive version is available at https://doi.org/10.1103/PhysRevA.52.2885

Coherent excitation of the singlet-triplet mixed $1s4f$ state of helium

J. B. Wang,[1] J. F. Williams,[1] A. T. Stelbovics,[2] J. E. Furst,[1] and D. H. Madison[3]
[1]*Centre for Atomic, Molecular and Surface Physics, Physics Department, University of Western Australia, Perth 6009, Australia*
[2]*School of Mathematical and Physical Sciences, Murdoch University, Perth 6150, Australia*
[3]*Laboratory for Atomic and Molecular Research, Missouri-Rolla University, Rolla, Missouri 65401*
(Received 15 December 1994)

In this paper, we present a detailed theoretical description for the coherent electron-impact excitation, the subsequent time evolution, and the cascading decay process of the singlet-triplet mixed $1s4f$ state of helium. The excitation amplitude and phase of each sublevel of this state are related to measurable coincidence intensities and polarizations of the emitted photons. It is found that the intensity and polarization of the emitted photons are time modulated due to the singlet and triplet mixing in the $1s4f$ state.

PACS number(s): 34.80.Dp

I. INTRODUCTION

The study of electron-atom collisions aims for a complete determination of all observables in the collision process, i.e., all quantum-mechanical excitation amplitudes and phases. The observation of coincidences between two or more of the outgoing particles (electrons and photons) from a collision complex is a prerequisite for obtaining such information. The associated theoretical work consists of two major parts. First, one solves the Schrödinger equation for a full description of the interactions between the projectile electron and the target atom; second, one establishes the time evolution of the excited atom after the collision and the subsequent decay processes.

Considerable progress has been made in approaching an accurate solution of the Schrödinger equation for describing particle collision processes, although it cannot be solved exactly even for the simplest collision systems. Many approximation methods have been developed over the past two decades, such as close-coupling theory including the R-matrix method, the optical-potential method in momentum space and the Kohn variational method; and perturbation theory including the plane-wave Born approximation, the distorted-wave Born approximation (DWBA), and the eikonal Born approximation. Examples of recent progress are the convergent-close-coupling calculation of Bray and Stelbovics [1], the second-order DWBA calculation of Madison, Bartschat, and McEachran [2], and the intermediate energy R-matrix calculation of Scott and Burke [3].

These theories are able to describe most measurements at small scattering angles in atomic hydrogen and helium when applied to the appropriate energy regions. As a general rule, the close-coupling theory works better for lower incident energies especially near threshold, while the perturbation theory provides good results for incident energies well above threshold. In this investigation, we have selected a particular incident energy of 100 eV, for which we would expect the first-order DWBA method to be quite accurate in calculating the amplitudes for the coherent excitation of $1s4f$ states of helium.

The time evolution and the sequential decay of the excited states can be modeled by using the general density-matrix theory developed by Fano and Macek [4] and Blum [5]. This theory provides a well-formulated description of the angular and polarization correlations for any electron-atom scattering experiments. For a few special cases, explicit formulas have been derived based on this theory, which directly connects the theoretical excitation amplitudes with experimental observables such as the intensity and polarization of the emitted photons [6–9]. These formulas are required in order to determine the optimum set of parameters to be measured in the minimum time and to make the most sensitive tests of atomic scattering theories.

However, studies have been limited to examining the excitation of the lowest few angular-momentum states. The main reasons for this limitation lies in the increased complexity of characterizing atoms with higher L. It becomes apparent when one begins to derive correlation functions for excitations beyond $L=1$ states that the expressions become rapidly intractable to analytic evaluation by conventional methods. This is due to the vast number of Clebsch-Gordan coefficients that comprise the correlation and polarization expressions, each of which is summed over several angular-momentum quantum numbers.

To illustrate the problems that can arise from this complexity, we consider the recent work for the angular correlations in electron-impact excitation of atomic hydrogen from the ground state to the $n=3$ states. In order to understand the excitation process of these states, coincidence measurements of (e,γ_1), (e,γ_2), (γ_1,γ_2), or (e,γ_1,γ_2) are needed. Here γ_1 is the Balmer-α photon emitted in the decay of the $3S$ and $3D$ states and γ_2 is the Lyman-α photons emitted from the $2P$ states. The report of the first study of the fluorescence from the decay of the $3\,^2D$ and $3\,^2S$ by Chwirot and Slevin [10] contained several errors in the derivation of angular correlation functions, which were corrected recently by Stelbovics, Kumar, and Williams [11]. The correction required substantial time and effort in cross-checking the angular-momentum algebra to ensure a correct final expression.

The study of even-odd parity coherence of $n=2$ states of hydrogen provides another example, for which Chwirot *et al.* [12] stressed that the most tedious part of the work involved algebraic manipulation of the correlation functions.

For the helium target, there is a further complication. The lowest angular-momentum states ($L \leq 2$) can be described adequately by the pure Russell-Saunders coupling scheme and their singlet and triplet states are well separated in energy. Detailed studies of the excitation processes to such states have been carried out by means of coincidence measurements [13–15]. However, for states with angular momentum $L \geq 3$, the LS coupling scheme breaks down. The physical reason for this can be seen in the following way. Consider singly excited configurations of helium atoms where one electron stays in its ground state. When the angular momentum of the helium atom increases, the excited electron moves further away from the nucleus and from the other electron. As a result, the exchange interaction between the two electrons decreases and the spin-orbit coupling becomes comparatively more important. Consequently, the total spin S is no longer a good quantum number and the use of a pure LS coupling scheme is invalid.

Nevertheless, since the pure LS-coupled eigenfunctions can be readily computed with existing computer softwares, the wave functions describing these mixed states are often described in terms of a linear combination of these LS-coupled eigenfunctions. For example, the $1s4f$ state of helium can be represented as a mixture of the singlet $4\,^1F_J$ and triplet $4\,^3F_J$ states. This state has shown rather different properties from those of the lower states with pure LS coupling as observed in ion-atom collisions [16,17]. It is worth noting that the total orbital angular momentum L of the atom equals that (l) of the excited outer electron and therefore is a good quantum number for singly excited helium atoms.

Parish and Mires [18] calculated the mixing coefficients for various states of helium using the Breit-Pauli Hamiltonian, which takes into account the Coulomb interaction, spin-orbit, spin-other-orbit, and spin-spin interactions between the two electrons. More sophisticated descriptions, which include relativistic and mass-polarization effects, were given by Cok and Lundeen [19,20] and Sims and Martin [21]. Experimental studies on the helium $1s4f$ state were carried out in proton-impact excitation by Kaiser, Liu, and von Oppen (see [17] and references therein) and in He-He and Na-He excitations by Liu *et al.* [22]. Their measured structure parameters, such as the level splitting and mixing coefficients, agree reasonably well with theoretical findings.

To our knowledge, however, little work has been done on the dynamics of the collision process involving excitation to the helium $1s4f$ state, particularly for electron-impact excitation. A complete understanding of such process would require measurements and calculations of the density matrix elements of this state, i.e., the population and interference of its magnetic sublevels, for various scattering angles and incident energies. The experimental limitations are (i) an electron energy resolution of about 0.1 eV is required to separate the $n=4$ and 5 levels, (ii) the photons emitted in the decay of the $1s4f$ state to the $3\,^1D$ and $3\,^3D$ states are 1870 and 1869 nm, respectively, which are not detectable by present single-particle counting photon detectors, and (iii) the long lifetime of about 67 nsec for the $1s4f$ state [23] also makes measurements difficult.

The purpose of this paper is to provide a definitive analysis of the density-matrix elements for the electron-impact excitation of the $1s4f$ state and subsequently to give some illustration of their applications. Thus, in the first part of this work, explicit formulas describing the intensity and polarization of the emitted photons in terms of the state multipoles of the excited $1s4f$ state are derived. In the second part, these state multipoles are evaluated using the DWBA method and finally some of the observables from coincidence measurements are modeled. These calculations aim to provide guidance for optimum experimental settings of the detectors for accessing the most efficient and revealing measurements.

II. THEORY

A. Definition of the $1s4f$ state multipoles

The Hamiltonian for a two-electron system may be written as

$$H=H_0+H_{\rm spin}+H_{\rm MP}+H_{\rm rel}\ , \tag{1}$$

where the Schrödinger Hamiltonian H_0 is about M_n/m_e times larger than the other terms, including $H_{\rm spin}=H_{\rm so_1}+H_{\rm so_2}+H_{\rm ss}$ for spin-orbit, spin-other-orbit, and spin-spin interactions, $H_{\rm MP}$ for mass polarization effect, and $H_{\rm rel}$ for relativistic corrections; M_n and m_e are the mass of the nucleus and the electron, respectively. Parish and Mires [18] neglected the $H_{\rm MP}$ and $H_{\rm rel}$ terms in the system Hamiltonian and took the LS-coupled wave function ($\phi^{S=1}_{m_s=1}$, $\phi^{S=1}_{m_s=0}$, $\phi^{S=1}_{m_s=-1}$, and $\phi^{S=0}_{m_s=0}$) as the basis states. They obtained

$$\Psi_k=a^t_{k,1}\phi^{S=1}_{m_s=1}+a^t_{k,0}\phi^{S=1}_{m_s=0}+a^t_{k,-1}\phi^{S=1}_{m_s=-1}+a^s_k\phi^{S=0}_{m_s=0}\ , \tag{2}$$

where the superscript t (s) indicates triplet (singlet) character and the indices $k=1,2,3$ correspond to the nominal "triplet" states with total angular momenta $J=L-1,L,L+1$ and $k=4$ refers to the nominal "singlet" state with $J=L$.

For the states with $J=L\pm1$ (i.e., $k=1,3$), only triplet LS eigenfunctions contribute. The associated coefficients $a^t_{k,i}$ are then equivalent to the Clebsch-Gordan coefficients $C(L=3,S=1,J;m_L m_S m_J)$. Therefore

$$|4\,^3F_{2m_J}\rangle\equiv|(L=3,\tilde{S}=1)J=2,m_J\rangle=|4\,^3F^o_{2m_J}\rangle\ , \tag{3}$$

$$|4\,^3F_{4m_J}\rangle\equiv|(L=3,\tilde{S}=1)J=4,m_J\rangle=|4\,^3F^o_{4m_J}\rangle\ , \tag{4}$$

where

$$|4\,^{2S+1}F^o_{Jm_J}\rangle=\sum_{m_L,m_S}C(L=3,S,J;m_L m_S m_J)\times|L=3,m_L;S,m_S\rangle\ , \tag{5}$$

the superscript o denotes the pure LS coupled states, and the spin index $\tilde{S} \equiv S$ in these two cases.

For states of $k=2,4$, the single and triplet levels are mixed and the calculated admixture coefficients are listed in Table VIII of Ref. [18]. van Raan and Heideman [24] made a considerable simplification to the wave functions for these states and gave them in the following form:

$$|4\,^1F_{3m_J}\rangle \equiv |(L=3,\tilde{S}=0)J=3,m_J\rangle = (|4\,^1F^o_{3m_J}\rangle + \omega|4\,^3F^o_{3m_J}\rangle)/\sqrt{1+\omega^2}\,, \tag{6}$$

$$|4\,^3F_{3m_J}\rangle \equiv |(L=3,\tilde{S}=1)J=3,m_J\rangle = (-\omega|4\,^1F^o_{3m_J}\rangle + |4\,^3F^o_{3m_J}\rangle)/\sqrt{1+\omega^2}\,. \tag{7}$$

In this way, only one admixture coefficient ω, instead of over 50 as listed in Ref. [18], is required for characterizing the mixed states. They estimated that $\omega=0.4335$ based on the results of Parish and Mires [18]. It is important to note that $(L\tilde{S})J$ does not refer to the Russell-Saunders pure LS coupling, but rather the intermediate coupling as defined by Eqs. (6) and (7). The state is largely a triplet state when the spin index $\tilde{S}=1$, whereas the state is largely a singlet state when $\tilde{S}=0$. Figure 1 shows the energy-level diagram of helium and the relevant decay schemes. The $2\,^1S$ state is not shown because the $2\,^1P \rightarrow 2\,^1S$ transition is very weak compared with $2\,^1P \rightarrow 1\,^1S$ and it provides essentially the same information.

In electron-impact excitation experiments, the four states $|4\,^3F_{2m_J}\rangle$, $|4\,^3F_{3m_J}\rangle$, $|4\,^3F_{4m_J}\rangle$, and $|4\,^1F_{3m_J}\rangle$ are in general indistinguishable with an average energy difference of $\sim$235 MHz [16] and their magnetic sublevels are degenerate in the absence of external fields. As a result, the $1s4f$ state is a statistical mixture of the sublevels denoted as $|(L\tilde{S})Jm_J\rangle$. Suppose that the atoms are initially in their ground state $|S_0=m_{S_0}=0\rangle$ and the incident electrons have fixed momentum $\mathbf{p}_0$ but are unpolarized in spin (m_{e0}). The density matrix of the combined system of electron and atom is $\rho_{\rm in}=\frac{1}{2}\sum_{m_{e0}}|m_{e0}\rangle\langle m_{e0}|$, where quantum numbers with fixed values are suppressed. After the collision, the density matrix becomes $\rho_{\rm out}=T\rho_{\rm in}T^\dagger$. If the scattered electrons are detected for fixed momentum $\mathbf{p}$ but no spin (m_e) analysis is performed, the density-matrix elements are

$$\sum_{m_e}\langle(L\tilde{S}')J'm'_Jm_e|\rho_{\rm out}|(L\tilde{S})J_{m_J}m_e\rangle = \tfrac{1}{2}\sum_{m_e,m_{e0}}\langle(L\tilde{S}')J'm'_Jm_e|T|m_{e0}\rangle \times\langle m_{e0}|T^\dagger|(L\tilde{S})Jm_Jm_e\rangle = \tfrac{1}{2}\sum_{m_e,m_{e0}} f((L\tilde{S}')J'm'_J,m_em_{e0})f^*((L\tilde{S})Jm_J,m_em_{e0}), \tag{8}$$

where the excitation amplitudes for the mixed states, according to Eqs. (3)–(7), are

$$f((L,\tilde{S}=0)J=3,m_Jm_em_{e0}) = [f_0(Jm_Jm_em_{e0})+\omega f_1(Jm_Jm_em_{e0})]/\sqrt{1+\omega^2}\,, \tag{9}$$

$$f((L,\tilde{S}=1)J=3,m_Jm_em_{e0}) = [-\omega f_0(Jm_Jm_em_{e0})+f_1(Jm_Jm_em_{e0})]/\sqrt{1+\omega^2}\,, \tag{10}$$

$$f((L,\tilde{S}=1)J=2,4,m_Jm_em_{e0}) = f_1(Jm_Jm_em_{e0})\,, \tag{11}$$

where $f_0(Jm_Jm_em_{e0})$ and $f_1(Jm_Jm_em_{e0})$ are, respectively, the pure singlet and pure triplet amplitudes for transitions $|n_0L_0m_{L0}S_0m_{S0};\vec{k}_{e0}m_{e0}\rangle \Longrightarrow |4\,^{2S+1}F^o_{Jm_J};\vec{k}_em_e\rangle$, $\vec{k}_{e0}$ and $\vec{k}_e$ are the momentum vector of the incident and scattered electrons, L_0 and S_0 are the orbital and spin angular momenta of the initial atomic state, m_{L0} and m_{S0} are the corresponding z components, n_0 is the principle quantum number of the initial state, and J and m_J denote the total angular momentum and its corresponding z component of the excited atomic state. These amplitudes are summed over the spins (m_{e0}, m_e) of both incident and scattered electrons and no electron-spin analysis is performed.

For calculations in relation to the angular and polarization correlations of the radiation field emitted by the excited atom, it is most convenient to use the state-multipole description defined as [5]

$$\langle T((L\tilde{S}')J'(L\tilde{S})J)^\dagger_{KQ}\rangle = \sum_{\substack{m'_J,m_J\\ m_e,m_{e0}}}(-1)^{J'-m'_J}\hat{K}\begin{pmatrix} J' & J & K\\ m'_J & -m_J & -Q\end{pmatrix} \times f((L\tilde{S}')J'm'_Jm_em_{e0}) \times f^*(L\tilde{S})Jm_Jm_em_{e0}) \tag{12}$$

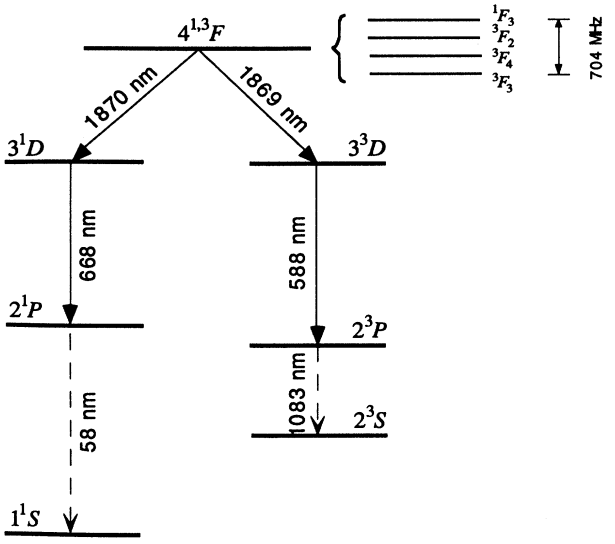

FIG. 1. Energy-level diagram and the relevant transition schemes.

because of the inherent symmetry in the excited atom. The notation $\hat{K}=\sqrt{2K+1}$ is used here and in the following.

From the above definition of state multipoles, we have

$$\langle T((L\tilde{S}')J'(L\tilde{S})J)^{\dagger}_{KQ}\rangle^{*} =(-1)^{J'-J+Q}\langle T((L\tilde{S})J(L\tilde{S}')J')^{\dagger}_{K-Q}\rangle \ . \quad (13)$$

In addition, the interaction of the electron-atom collision possesses reflection invariance in the scattering plane and thus the scattering amplitudes defined in the collision frame must satisfy the condition [25]

$$f((L\tilde{S})Jm_J m_e m_{e0})=(-1)^{L+J-m_J+1/2-m_e+1/2-m_{e0}} \times f((L\tilde{S})J-m_J-m_e-m_{e0}) \ . \quad (14)$$

This gives

$$\langle T((L\tilde{S}')J'(L\tilde{S})J)^{\dagger}_{KQ}\rangle =(-1)^{K+Q}\langle T((L\tilde{S}')J'(L\tilde{S})J)^{\dagger}_{K-Q}\rangle \ . \quad (15)$$

From Eqs. (13) and (15), we have

$$\langle T((L\tilde{S}')J'(L\tilde{S})J)^{\dagger}_{KQ}\rangle =(-1)^{J'-J+K}\langle T((L\tilde{S})J(L\tilde{S}')J')^{\dagger}_{KQ}\rangle^{*} \ . \quad (16)$$

A further symmetry

$$\langle T((L\tilde{S}')J(L\tilde{S})J)^{\dagger}_{KQ}\rangle=\langle T((L\tilde{S})J(L\tilde{S}')J)^{\dagger}_{KQ}\rangle \quad (17)$$

is also found when $J'=J$, which is due to summing over both final and initial electron spins in the state multipoles as defined by Eq. (12).

B. Evaluation of the transition amplitudes

In order to obtain the values for the $1s4f$ state multipoles defined by Eq. (12), we first calculate the pure singlet and triplet excitation amplitudes in the DWBA [26]

$$f_S(Jm_J m_e m_{e0})=\langle \vec{k}_e m_e\,{}^{2S+1}\bar{F}_{Jm_J}|T|\vec{k}_{e0}\tfrac{1}{2}m_{e0},J_0=m_{J_0}=0\rangle = \sum_{\substack{m_L,m_S\\ S_T,m_{S_T}}} C(LSJ;m_L m_S m_J)C(S\tfrac{1}{2}S_T;m_S m_e m_{S_T})\langle \vec{k}_e,Lm_L|T|\vec{k}_{e0},L_0=m_{L_0}=0\rangle_S \delta_{S_T,1/2}\delta_{m_{S_T},m_{e0}} \ , \quad (18)$$

where T is the standard T matrix operator, $C(\ )$ are the Clebsch-Gordan coefficients, S_T denotes the total spin of the target plus projectile electron system, and m_{S_T} is its z component. These excitation amplitudes depend on the collision dynamics, the energy of the incident electron, and the angular momentum transferred to the atom, as well as the spin states of the continuum electron. It is usually assumed that, in the case of light atoms, there are no spin-dependent forces in the T operator and no relativistic forces for the continuum electron. Therefore, the total spin S_T and its z component m_{S_T} are conserved after the collision.

The heart of the task is to calculate the transition matrix elements in the above equation, where each basis state is of Russell-Saunders coupling scheme. The DWBA transition matrix elements are [27]

$$\langle \vec{k}_e,Lm_L|T|\vec{k}_{e0},L_0=m_{L_0}=0\rangle_S =\sqrt{2}\langle \phi_1^{-}(0)\psi_{nLm_L}(1)|V|\phi_0^{+}(0)\psi_{1s}(1)\rangle\delta_{S,0} - \left[\frac{2S+1}{2}\right]^{1/2}(-1)^S \times\langle \phi_1^{-}(1)\psi_{nLm_L}(0)|V|\phi_0^{+}(0)\psi_{1s}(1)\rangle \ , \quad (19)$$

where ϕ_0^{+} and ϕ_1^{-} are the spatial parts of the incident and scattered distorted waves with appropriate boundary conditions, ψ_0 and ψ_{nLm} are coordinate-space single-particle wave functions of the ground and excited state of the

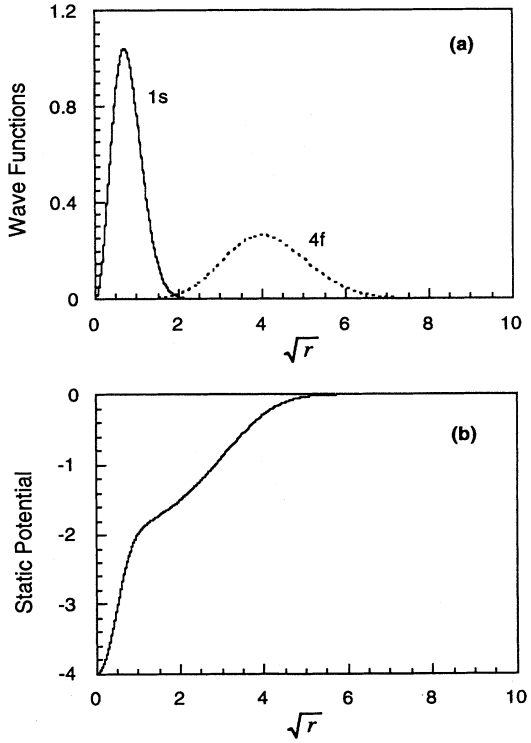

FIG. 2. (a) Target radial wave functions for the $1s$ and $4f$ orbitals and (b) the corresponding excited-state static potential shown as rU_f.

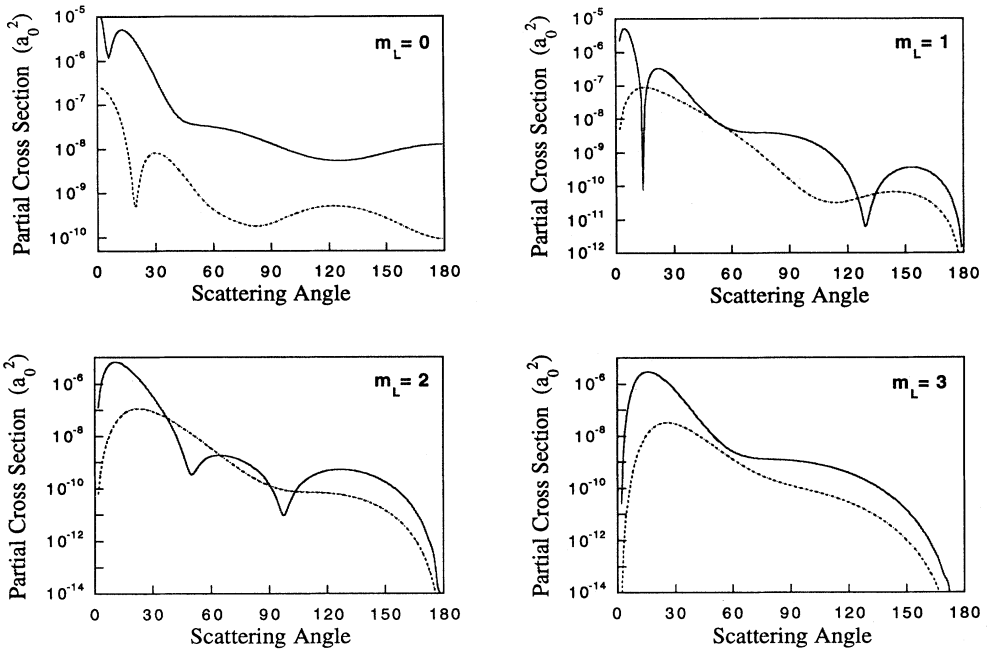

FIG. 3. Calculated results of the partial cross sections defined as $(\sigma^S_{m_L} = |\langle \vec{k}_e, Lm_L | T | \vec{k}_{e0}, L_0 = m_{L0} = 0 \rangle_S|^2$ for an electron incident energy of 100 eV. Solid lines, singlet state $S=0$; dashed lines, triplet state $S=1$.

helium atom, and V is the full interaction potential between the continuum electron and the atom. The first and the second term refer to the direct and the exchange amplitude, respectively.

The distorted waves are solutions of the equation

$$(\nabla^2 + k^2 - U)\phi = 0 , \tag{20}$$

where k^2 is the energy of the incident electron and U is the distorting potential obtained from the charge distribution of the atomic wave functions. The spatial atomic wave functions obtained from the Hartree-Fock program of Froese Fisher [28] are shown in Fig. 2(a). According to Bartschat and Madison [27], the best agreement with experimental data was obtained when both the initial- and the final-state distorted waves were calculated using the excited-state potential U_f, which is shown in Fig. 2(b) as rU_f. In Fig. 3 we display the calculated results for the partial cross sections defined as $\sigma^S_{m_L} = |\langle \vec{k}_e, Lm_L | T | \vec{k}_{e0}, L_0 = m_{L0} = 0 \rangle_S|^2$. The calculations were done for the electron incident energy of 100 eV and various scattering angles. The integrated total cross section is found to be $1.1 \times 10^{-5} a_0^2$ for excitation to the pure $4\,^1F^o$ state and $6.0 \times 10^{-7} a_0^2$ to the pure $4\,^3F^o$ state.

The values of the transition matrix elements $\langle \vec{k}_e, Lm_L | T | \vec{k}_{e0}, L_0 = m_{L_0} = 0 \rangle_S$ were then used to compute the excitation amplitudes $f((L\tilde{S})Jm_J)$ and the corresponding state multipoles $\langle T((L\tilde{S}')J'(L\tilde{S})J)^\dagger_{KQ} \rangle$, which characterize the coherently mixed $1s4f$ state immediately after electron-impact excitation. Equations (18), (9)–(11), and (13) are applied for such computations. The results are listed in Tables I–V for $\langle T(\tilde{S}'_3 \tilde{S}_3)^\dagger_{KQ} \rangle \equiv \langle T((L\tilde{S}')J'(L\tilde{S})J)^\dagger_{KQ} \rangle|_{L=J'=J=3}$ with ranks $K \leq 2$. The calculations were done for two cases with the admixture coefficient $\omega = 0$ and 0.4335, respectively. Note that $\langle T(\tilde{S}'_3 = 0, \tilde{S}_3 = 1)^\dagger_{KQ} \rangle \equiv 0$ in the case of $\omega = 0$.

C. Time evolution of the state multipoles and the subsequent decay process

After collision, the excited atom evolves under its system Hamiltonian and decays at some finite time to a lower state while emitting a photon with specific wavelength. This procedure repeats until the atom decays to

TABLE I. Calculated values of the state multipoles $\langle T(\tilde{S}'_3 = \tilde{S}_3 = 0)^\dagger_{KQ} \rangle$ for $\omega = 0.0$.

Angle (deg)	T_{00}	T_{10}	T_{11}	T_{20}	T_{21}	T_{22}
10	16.8	0	$-2.45I$	−2.84	−11	−6.83
20	11	0	$1.19I$	1.96	−5.05	−6.88
30	2.23	0	$0.473I$	0.469	−0.763	−1.46
40	0.293	0	$0.129I$	0.023 1	−0.054 3	−0.179
50	0.062 3	0	$0.042\,6I$	−0.027 4	0.004 2	−0.032 6
60	0.038	0	$0.020\,4I$	−0.029 6	0.004 75	−0.021 8
70	0.030 5	0	$0.013\,9I$	−0.025 3	0.003 75	−0.018 6
80	0.023 7	0	$0.011\,3I$	−0.019 7	0.003 28	−0.013 9
90	0.017 5	0	$0.009\,23I$	−0.014 2	0.002 75	−0.008 9

TABLE II. Calculated values of the state multipoles $\langle T(\tilde{S}'_3=\tilde{S}_3=1)^{\dagger}_{KQ}\rangle$ for $\omega=0.0$.

Angle (deg)	T_{00}	T_{10}	T_{11}	T_{20}	T_{21}	T_{22}
10	0.074 7	0	$-0.005\,65I$	−0.047 2	−0.031 8	0.005 75
20	0.11	0	$0.010\,2I$	−0.017 4	−0.067 5	−0.006 61
30	0.09	0	$0.013\,2I$	−0.003 16	−0.053 2	−0.014 4
40	0.041 7	0	$0.006\,23I$	−0.002 29	−0.024	−0.007 51
50	0.015 2	0	$0.001\,93I$	−0.001 87	−0.008 45	−0.002 62
60	0.005 21	0	$0.000\,435I$	−0.001 03	−0.002 7	−0.000 81
70	0.001 77	0	$0.000\,046\,8I$	−0.000 416	−0.000 82	−0.000 233
80	0.000 631	0	$0.000\,00I$	−0.000 131	−0.000 24	−0.000 072 3
90	0.000 28	0	$0.000\,017\,6I$	−0.000 043 9	−0.000 077 8	−0.000 045 4

TABLE III. Calculated values of the state multipoles $\langle T(\tilde{S}'_3=\tilde{S}_3=0)^{\dagger}_{KQ}\rangle$ for $\omega=0.4335$.

Angle (deg)	T_{00}	T_{10}	T_{11}	T_{20}	T_{21}	T_{22}
10	14.2	0	$-2.06I$	−2.4	−9.27	−5.75
20	9.32	0	$1.0I$	1.65	−4.26	−5.79
30	1.89	0	$0.4I$	0.394	−0.651	−1.23
40	0.253	0	$0.11I$	0.019	−0.049 5	−0.152
50	0.054 9	0	$0.036\,2I$	−0.023 3	0.002 2	−0.027 8
60	0.032 8	0	$0.017\,2I$	−0.025 1	0.003 57	−0.018 5
70	0.026	0	$0.011\,7I$	−0.021 4	0.003 03	−0.015 7
80	0.020 1	0	$0.009\,5I$	−0.016 6	0.002 72	−0.011 7
90	0.014 7	0	$0.007\,77I$	−0.012	0.002 31	−0.007 5

TABLE IV. Calculated values of the state multipoles $\langle T(\tilde{S}'_3=0,\tilde{S}_3=1)^{\dagger}_{KQ}\rangle$ for $\omega=0.4335$.

Angle (deg)	T_{00}	T_{10}	T_{11}	T_{20}	T_{21}	T_{22}
10	−6.1	0	$0.089\,1I$	1.02	4	2.49
20	−3.99	0	$-0.43I$	−0.721	1.82	2.51
30	−0.78	0	$-0.168I$	−0.172	0.259	0.529
40	−0.091 6	0	$-0.044\,9I$	−0.009 25	−0.011 1	0.062 5
50	−0.017 2	0	$-0.014\,8I$	0.009 31	−0.004 62	0.010 9
60	−0.012	0	$-0.007\,28I$	0.010 4	−0.002 72	0.007 65
70	−0.010 5	0	$-0.005\,07I$	0.009 09	−0.001 67	0.006 69
80	−0.008 42	0	$-0.004\,12I$	0.007 13	−0.001 28	0.005 03
90	−0.006 27	0	$-0.003\,36I$	0.005 17	−0.001 03	0.003 23

TABLE V. Calculated values of the state multipoles $\langle T(\tilde{S}'_3=\tilde{S}_3=1)^{\dagger}_{KQ}\rangle$ for $\omega=0.4335$.

Angle (deg)	T_{00}	T_{10}	T_{11}	T_{20}	T_{21}	T_{22}
10	2.72	0	$-0.392I$	−0.489	−1.77	−1.08
20	1.84	0	$0.196I$	0.295	−0.856	−1.09
30	0.428	0	$0.085\,9I$	0.071 5	−0.166	−0.244
40	0.081 4	0	$0.025\,7I$	0.001 72	−0.028 8	−0.034 6
50	0.022 7	0	$0.008\,36I$	−0.005 9	−0.006 45	−0.007 35
60	0.010 4	0	$0.003\,59I$	−0.005 54	−0.001 52	−0.004 12
70	0.006 32	0	$0.002\,24I$	−0.004 36	−0.000 096	−0.003 13
80	0.004 28	0	$0.001\,78I$	−0.003 22	0.000 316	−0.002 25
90	0.003	0	$0.001\,48I$	−0.002 29	0.000 37	−0.001 45

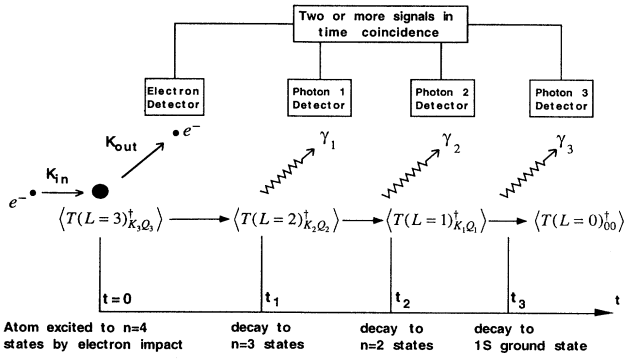

FIG. 4. Time evolution of the excited atom and sequential cascading scheme.

its ground state. The angular distribution and polarization of the emitted photons are fully determined by the state multipoles of the excited atom immediately after collision. In this section, we aim to establish such relationships.

The time evolution of the excited atom and the cascading decay processes are depicted in Fig. 4. Also shown are the possible observations of a variety of coincidence events. The electron-impact excitation of the $1s4f$ state takes place at $t=0$. After the collision, the excited atom described by $\langle T((L_3\tilde{S}')J'_3(L_3\tilde{S})J_3)^\dagger_{K_3Q_3}\rangle$ evolves with time until $t=t_1$. It then decays to either the $3\,^1D$ or the $3\,^3D$ state represented, respectively, by $\langle T((L=2,S=0)J_2)^\dagger_{K_2Q_2}\rangle$ and $\langle T((L=2,S=1)J'_2J_2)^\dagger_{K_2Q_2}\rangle$. The $3\,^1D$ [$3\,^3D$] state evolves further with time until the second photon is emitted at $t=t_2$ and the atom decays to the $2\,^1P$ [$2\,^3P$] state represented by $\langle T((L=1,S=0)J_1)^\dagger_{K_1Q_1}\rangle$ [$\langle T((L=1,S=1)J'_1J_1)^\dagger_{K_1Q_1}\rangle$]. Finally, the atom emits the third photon at $t=t_3$ and decays to the monopole state $1\,^1S$ [$2\,^3S$].

An analysis of this sequential cascade process requires three basic equations. The first equation describes the time evolution of the excited atom, the second equation gives the spatial distribution and polarization state of the emitted photon from such a state, and the third equation provides the configuration of the lower state of the atom immediately after emitting the photon. The derivation of these three equations is given below, which follows closely the general density-matrix theory presented by Blum [5].

The density matrix of the excited $1s4f$ state immediately after the collision is

$$\rho(0)=\sum_{\substack{J'_3J_3,\tilde{S}'_3,\tilde{S}'_3\\K_3,Q_3}}\langle T((L_3,\tilde{S}'_3)J'_3(L_3,\tilde{S}_3)J_3)^\dagger_{K_3Q_3}\rangle \times T((L_3,\tilde{S}'_3)J'_3(L_3\tilde{S}_3)J_3)_{K_3Q_3}\,. \tag{21}$$

The excited atom evolves with time in the total angular momentum space $|Jm_J\rangle$ and the corresponding time-dependent density matrix is

$$\rho(t)=U(t)\rho(0)U(t)^\dagger\,, \tag{22}$$

where $U(t)=e^{-iHt/\hbar}$ is the time evolution operator and H is the system Hamiltonian of the target atom. We then obtain the time dependence of the $1s4f$ state multipoles as

$$\begin{aligned}\langle T((L_3\tilde{S}'_3)J'_3(L_3\tilde{S}_3)J_3;t)^\dagger_{k_3q_3}\rangle &=\mathrm{Tr}\{\rho(t)T((L_3\tilde{S}'_3)J'_3(L_3\tilde{S}_3)J_3)^\dagger_{k_3q_3}\}\\ &=\sum_{K_3,Q_3}\langle T((L_3\tilde{S}'_3)J'_3(L_3\tilde{S}_3)J_3)^\dagger_{K_3Q_3}\rangle\mathrm{Tr}\{U(t)T((L_3\tilde{S}'_3)J'_3(L_3\tilde{S}_3)J_3)_{K_3Q_3}U(t)^\dagger T((L_3,\tilde{S}'_3)J'_3(L_3\tilde{S}_3)J_3)^\dagger_{k_3q_3}\}\,,\end{aligned} \tag{23}$$

where

$$\mathrm{Tr}\{\cdots\}\equiv G((L_3\tilde{S}'_3)J'_3(L_3\tilde{S}_3)J_3;t)=e^{-\gamma_3-i(E_{(L_3\tilde{S}_3)J_3}-E_{(L_3\tilde{S}'_3)J'_3})t/\hbar}\delta_{K_3k_3}\delta_{Q_3q_3} \tag{24}$$

is the time evolution coefficient, $(E_{J_i}-E_{J'_i})$ are the energy splitting of the four sublevels of the $1s4f$ state, and γ_3 is the radiative decay rate of this state.

The next step is to derive the density matrix of the first photon (γ_1) emitted at $t=t_1$, which will contain all information about the spatial distribution and polarization state of this photon. In dipole approximation, this is

$$\rho(\lambda'_1\lambda_1\vec{n}_1;t_1)=C(\omega_1)\sum_{\substack{K_3,q_3,Q_3\\J_3,J'_3,\tilde{S}_3,\tilde{S}'_3}}\langle T((L_3\tilde{S}'_3)J'_3(L_3\tilde{S}_3)J_3;t_1)^\dagger_{K_3Q_3}\rangle^{\mathrm{lab}}D(0\theta_1\varphi_1)^{K_3}_{q_3Q_3} \times\mathrm{Tr}\{r_{-\lambda'_1}T((L_3,\tilde{S}'_3)J'_3(L_3\tilde{S}_3)J_3)_{K_3q_3}r^\dagger_{-\lambda_1}\}^{\vec{n}_1}\,, \tag{25}$$

where λ, ω, and $\vec{n}\equiv(\theta,\varphi)$ denote the helicity, frequency, and Euler angles of the emitted photon, $C(\omega)=e^2\omega^2d\Omega/2\pi c^3\hbar$, and lab refers to the laboratory frame in which θ and φ are defined. The trace in the above equation is

$$\mathrm{Tr}\{\cdots\}=\sum_{J_2}(-1)^{J_2+J_3+\lambda_1}\hat{K}_3\begin{Bmatrix}1 & 1 & K_3\\ -\lambda_1' & \lambda_1 & q_3\end{Bmatrix}\begin{Bmatrix}1 & 1 & K_3\\ J_3 & J_3' & J_2\end{Bmatrix}(\hat{J}_2)^2\hat{J}_3\hat{J}_3'|\langle L_2\|\vec{r}\|L_3\rangle|^2$$
$$\times\left[\omega^0_{\tilde{S}_3'J_3'}\omega^0_{\tilde{S}_3J_3}\begin{Bmatrix}L_2 & J_2 & 0\\ J_3' & L_3 & 1\end{Bmatrix}\begin{Bmatrix}L_2 & J_2 & 0\\ J_3 & L_3 & 1\end{Bmatrix}\delta_{S_20}+\omega^1_{\tilde{S}_3'J_3'}\omega^1_{\tilde{S}_3J_3}\begin{Bmatrix}L_2 & J_2 & 1\\ J_3' & L_3 & 1\end{Bmatrix}\begin{Bmatrix}L_2 & J_2 & 1\\ J_3 & L_3 & 1\end{Bmatrix}\delta_{S_21}\right], \quad (26)$$

where $\omega^0_{1,2}=\omega^0_{1,4}=0$, $\omega^1_{1,2}=\omega^1_{1,4}=1$, $\omega^0_{0,3}=\omega^1_{1,3}=1/\sqrt{1+\omega^2}$, and $\omega^1_{0,3}=-\omega^0_{1,3}=\omega/\sqrt{1+\omega^2}$. The lower state $3\,^1D$ [$3\,^3D$] of the atom immediately after the emission of the first photon can be represented by its state multipoles

$$\langle T((L_2S_2)J_2'J_2;t_1)^\dagger_{K_2Q_2}\rangle^{\mathrm{lab}}=C(\omega_1)\sum_{\substack{K_3,q_3,Q_3,q_2\\ J_3,J_3',\tilde{S}_3,\tilde{S}_3'}}\langle T((L_3\tilde{S}_3')J_3'(L_3\tilde{S}_3)J_3;t_1)^\dagger_{K_3Q_3}\rangle^{\mathrm{lab}}D(0\theta_1\varphi_1)^{K_3}_{q_3Q_3}$$
$$\times\mathrm{Tr}\{r_{-\lambda_1'}T((L_3\tilde{S}_3')J_3'(L_3\tilde{S}_3)J_3)_{K_3q_3}$$
$$\times r^\dagger_{-\lambda_1'}T((L_2S_2)J_2'J_2)^\dagger_{K_2q_2}\}^{\vec{n}_1}D^*(0\theta_1\varphi_1)^{K_2}_{q_2Q_2}, \quad (27)$$

where the trace

$$\mathrm{Tr}\{\cdots\}=(-1)^{K_3+q_2+J_3+J_3'}\hat{K}_2\hat{K}_3(\hat{J}_2)^2\hat{J}_3\hat{J}_3'|\langle L_2\|\vec{r}\|L_3\rangle|^2$$
$$\times\left[\omega^0_{\tilde{S}_3'J_3'}\omega^0_{\tilde{S}_3J_3}\begin{Bmatrix}L_2 & J_2' & 0\\ J_3' & L_3 & 1\end{Bmatrix}\begin{Bmatrix}L_2 & J_2 & 0\\ J_3 & L_3 & 1\end{Bmatrix}\delta_{S_20}+\omega^1_{\tilde{S}_3'J_3'}\omega^1_{\tilde{S}_3J_3}\begin{Bmatrix}L_2 & J_2' & 1\\ J_3' & L_3 & 1\end{Bmatrix}\begin{Bmatrix}L_2 & J_2 & 1\\ J_3 & L_3 & 1\end{Bmatrix}\delta_{S_21}\right]$$
$$\times\sum_b(2b+1)\begin{bmatrix}K_3 & b & K_2\\ q_3 & (\lambda_1'-\lambda_1) & -q_2\end{bmatrix}\begin{bmatrix}b & 1 & 1\\ (\lambda_1-\lambda_1') & \lambda_1' & -\lambda_1\end{bmatrix}\begin{Bmatrix}K_3 & b & K_2\\ J_3 & 1 & J_2\\ J_3' & 1 & J_2'\end{Bmatrix}. \quad (28)$$

Detailed calculations of the various traces [Eqs. (24), (26), and (28)] are given in the Appendix. The above equations also apply to the subsequent time evolution and decay of the atom, except that the lower states are well represented by the pure LS-coupling scheme and the traces will have simpler forms. The density matrix of the second photon (γ_2) is, in the dipole approximation,

$$\rho(\lambda_1'\lambda_1\vec{n}_1,\lambda_2'\lambda_2\vec{n}_2;t_1,t_2)=C(\omega_2)\sum_{\substack{K_2,q_2',Q_2\\ J_2,J_2'}}\langle T((L_2S_2)J_2'J_2;t_1)^\dagger_{K_2Q_2}\rangle^{\mathrm{lab}}D(0\theta_2\varphi_2)^{K_2}_{q_2'Q_2}$$
$$\times G((L_2S_2)J_2'J_2;(t_2-t_1))\mathrm{Tr}\{r_{-\lambda_2'}T((L_2S_2)J_2'J_2)_{K_2q_2'}r^\dagger_{-\lambda_2}\}^{\vec{n}_2}, \quad (29)$$

where

$$\mathrm{Tr}\{\cdots\}\equiv\sum_{J_1}(-1)^{J_1+J_2'+\lambda_2}\begin{Bmatrix}1 & 1 & K_2\\ -\lambda_2' & \lambda_2 & q_2'\end{Bmatrix}\begin{Bmatrix}1 & 1 & K_2\\ J_2 & J_2' & J_1\end{Bmatrix}\hat{K}_2$$
$$\times(\hat{J}_1)^2\hat{J}_2\hat{J}_2'\begin{Bmatrix}L_1 & J_1 & S_1\\ J_2 & L_2 & 1\end{Bmatrix}\begin{Bmatrix}L_1 & J_1 & S_1\\ J_2' & L_2 & 1\end{Bmatrix}\delta_{S_1S_2}|\langle L_1\|\vec{r}\|L_2\rangle|^2 \quad (30)$$

and the state multipoles of the $2\,^1P$ [$2\,^3P$] state immediately after the emission of the second photon is

$$\langle T((L_1S_1)J_1'J_1;t_1t_2)^\dagger_{K_1Q_1}\rangle^{\mathrm{lab}}$$
$$=C(\omega_2)\sum_{\substack{K_2,q_2',Q_2q_1\\ J_2,J_2'}}\langle T((L_2S_2)J_2'J_2;t_1)^\dagger_{K_2Q_2}\rangle^{\mathrm{lab}}D(0\theta_2\varphi_2)^{K_2}_{q_2'Q_2}G((L_2S_2)J_2'J_2;(t_2-t_1))$$
$$\times\mathrm{Tr}\{r_{-\lambda_2'}T((L_2S_2)J_2'J_2)_{K_2q_2'}r^\dagger_{-\lambda_2}T((L_1S_1)J_1'J_1)^\dagger_{K_1q_1}\}^{\vec{n}_2}D^*(0\theta_2\varphi_2)^{K_1}_{q_1Q_1}, \quad (31)$$

where

$$\mathrm{Tr}\{\cdots\}\equiv(-1)^{J_2+J_2'+K_2+q_1}\hat{K}_1\hat{K}_2\hat{J}_1'\hat{J}_1\hat{J}_2'\hat{J}_2\begin{Bmatrix}L_1 & J_1 & S_1\\ J_2 & L_2 & 1\end{Bmatrix}\begin{Bmatrix}L_1 & J_1' & S_1\\ J_2' & L_2 & 1\end{Bmatrix}\delta_{S_1S_2}|\langle L_1\|\vec{r}\|L_2\rangle|^2$$

$$\times\sum_{b'}(2b'+1)\begin{bmatrix}K_2 & b' & K_1\\ q_2' & (\lambda_2'-\lambda_2) & -q_1\end{bmatrix}\begin{bmatrix}b' & 1 & 1\\ (\lambda_2-\lambda_2') & \lambda_2' & -\lambda_2\end{bmatrix}\begin{bmatrix}K_2 & b' & K_1\\ J_2 & 1 & J_1\\ J_2' & 1 & J_1'\end{bmatrix}. \tag{32}$$

Finally, the density matrix of the third photon (γ_3) is

$$\rho(\lambda_1'\lambda_1\vec{n}_1,\lambda_2'\lambda_2\vec{n}_2,\lambda_3'\lambda_3\vec{n}_3;t_1,t_2,t_3)=C(\omega_3)\sum_{\substack{K_1,q_1',Q_1\\ J_1,J_1'}}\langle T((L_1S_1)J_1'J_1;t_1t_2)^{\dagger}_{K_1Q_1}\rangle^{\mathrm{lab}}D(0\theta_3\varphi_3)^{K_1}_{q_1'Q_1}G((L_1S_1)J_1'J_1;(t_3-t_2))$$

$$\times\mathrm{Tr}\{r_{-\lambda_3'}T((L_1S_1)J_1'J_1)_{K_1q_1'}r^{\dagger}_{-\lambda_3}\}^{\vec{n}_3}, \tag{33}$$

where

$$\mathrm{Tr}\{\cdots\}\equiv\sum_{J_0}(-1)^{J_0+J_1'+\lambda_3}\begin{bmatrix}1 & 1 & K_1\\ -\lambda_3' & \lambda_3 & q_1'\end{bmatrix}$$

$$\times\begin{Bmatrix}1 & 1 & K_1\\ J_1 & J_1' & J_0\end{Bmatrix}\hat{K}_1(\hat{J}_0)^2\hat{J}_1\hat{J}_1'$$

$$\times\begin{Bmatrix}L_0 & J_0 & S_0\\ J_1 & L_1 & 1\end{Bmatrix}\begin{Bmatrix}L_0 & J_0 & S_0\\ J_1' & L_1 & 1\end{Bmatrix}$$

$$\times\delta_{S_0S_1}|\langle L_0\|\vec{r}\|L_1\rangle|^2. \tag{34}$$

The atom then decays to the monopole $1\,^1S\,[2\,^3S]$ state.

III. CASE STUDY

A complete determination of all $1s4f$ state multipoles up to rank 6 would require measurements and analysis of the three-photon density matrix given by Eq. (33). This can be achieved by measuring the coincidence rates between the scattered electron and the three cascading photons for a set of polarization and angular correlations. However, detection of quadruple coincidences will have to await further advance of experimental techniques and it is unlikely to become feasible in the foreseeable future. Nevertheless, we are able to attain most information on the $1s4f$ state, especially the mixing characteristics of this state, by measuring and analyzing one or two of the transitions shown in Fig. 1.

A. Explicit formulas for the $1s4f\rightarrow 3\,^1D$ transition

As discussed earlier, the excited $1s4f$ state decays, after some finite time, to either the $3\,^1D$ or the $3\,^3D$ state. Photons emitted from these two transitions (with wavelengths of 1870 and 1869 nm, respectively) are not correlated in time or phase, because they are related to two separate lower states. Nevertheless, both photons reflect the mixed nature of the $1s4f$ state. In other words, the intensity and polarizations of either photon are functions of the admixture coefficient ω.

For simplicity, we consider the transition $1s4f\rightarrow 3\,^1D$, where $S_2=0$ and $J_2=J_2'=L_2=2$. The explicit density matrix of the emitted photon can be readily obtained by substituting Eq. (26) into Eq. (25),

$$\rho(\lambda_1'\lambda_1\vec{n}_1;t)=C_1\sum_{\substack{K_3,q_3,Q_3\\ \tilde{S}_3,\tilde{S}_3'}}(-1)^{\lambda_1}\hat{K}_3\begin{bmatrix}1 & 1 & K_3\\ -\lambda_1' & \lambda_1 & q_3\end{bmatrix}\begin{Bmatrix}1 & 1 & K_3\\ J_3 & J_3' & J_2\end{Bmatrix}\omega^0_{\tilde{S}_3'3}\omega^0_{\tilde{S}_33}$$

$$\times\langle T((L_3\tilde{S}_3')J_3'(L_3\tilde{S}_3)J_3)^{\dagger}_{K_3Q_3}\rangle^{\mathrm{lab}}D(0\theta_1\varphi_1)^{K_3}_{q_3Q_3}e^{-\gamma_3 t}\cos[(E_{\tilde{S}_3'}-E_{\tilde{S}_3})t/\hbar], \tag{35}$$

where $C_1=(-1)^{J_2+J_3}(\hat{J}_2\hat{J}_3|\langle L_2\|\vec{r}\|L_3\rangle|)^2C(\omega_1)$. Note that in this case the trace in Eq. (26) is nonnzero only if $J_3=J_3'=L_3=3$.

The coincidence intensity and the Stokes parameters are defined as the various combinations of the two-photon density matrix. They are evaluated using an algebraic package written in MATHEMATICA [29]. The results are

$$I(\theta\varphi;t)=\rho(\lambda_1'=1,\lambda_1=1)+\rho(\lambda_1'=-1,\lambda_1=-1)$$
$$=C_1\sum_{\tilde{S}_3',\tilde{S}_3}\omega^0_{\tilde{S}_3'3}\omega^0_{\tilde{S}_3 3}e^{-\gamma_3 t}\cos[(E_{\tilde{S}_3'}-E_{\tilde{S}_3})t/\hbar]$$
$$\times\left\{\frac{2}{3\sqrt{7}}\langle T(\tilde{S}_3'\tilde{S}_3)^\dagger_{00}\rangle+\frac{1}{10\sqrt{21}}(1+3\cos2\theta)\langle T(\tilde{S}_3'\tilde{S}_3)^\dagger_{20}\rangle\right.$$
$$\left.+\frac{1}{5}\left[\frac{2}{7}\right]^{1/2}[\cos2\varphi\sin^2\theta\langle T(\tilde{S}_3'\tilde{S}_3)^\dagger_{22}\rangle-\cos\varphi\sin2\theta\langle T(\tilde{S}_3'\tilde{S}_3)^\dagger_{21}\rangle]\right\}, \tag{36}$$

$$IP_1(\theta\varphi;t)=-[\rho(\lambda_1'=1,\lambda_1=-1)+\rho(\lambda_1'=-1,\lambda_1=1)]$$
$$=C_1\sum_{\tilde{S}_3',\tilde{S}_3}\omega^0_{\tilde{S}_3'3}\omega^0_{\tilde{S}_3 3}e^{-\gamma_3 t}\cos[(E_{\tilde{S}_3'}-E_{\tilde{S}_3})t/\hbar]$$
$$\times\left\{-\frac{1}{5}\left[\frac{3}{7}\right]^{1/2}\sin^2\theta\langle T(\tilde{S}_3'\tilde{S}_3)^\dagger_{20}\rangle-\frac{1}{5}\left[\frac{2}{7}\right]^{1/2}\cos\varphi\sin2\theta\langle T(\tilde{S}_3'\tilde{S}_3)^\dagger_{21}\rangle\right.$$
$$\left.-\frac{1}{5\sqrt{14}}\cos2\varphi(3+\cos2\theta)\langle T(\tilde{S}_3'\tilde{S}_3)^\dagger_{22}\rangle\right\}, \tag{37}$$

$$IP_2(\theta\varphi;t)=-i[\rho(\lambda_1'=1,\lambda_1=-1)-\rho(\lambda_1'=-1,\lambda_1=1)]$$
$$=C_1\sum_{\tilde{S}_3'\tilde{S}_3}\omega^0_{\tilde{S}_3'3}\omega^0_{\tilde{S}_3 3}e^{-\gamma_3 t}\cos[(E_{\tilde{S}_3'}-E_{\tilde{S}_3})t/\hbar]\frac{2}{5}\left[\frac{2}{7}\right]^{1/2}\{\sin\varphi\sin\theta\langle T(\tilde{S}_3'\tilde{S}_3)^\dagger_{21}\rangle+\sin2\varphi\cos\theta\langle T(\tilde{S}_3'\tilde{S}_3)^\dagger_{22}\rangle\}, \tag{38}$$

$$IP_3(\theta\varphi;t)=\rho(\lambda_1'=-1,\lambda_1=-1)-\rho(\lambda_1'=1,\lambda_1=1)$$
$$=C_1\sum_{\tilde{S}_3',\tilde{S}_3}\omega^0_{\tilde{S}_3'3}\omega^0_{\tilde{S}_3 3}e^{-\gamma_3 t}\cos[(E_{\tilde{S}_3'}-E_{\tilde{S}_3})t/\hbar]\frac{2}{3\sqrt{7}}\{-\cos\theta\langle T(\tilde{S}_3'\tilde{S}_3)^\dagger_{10}\rangle-\sqrt{2}\sin\varphi\sin\theta\,\mathrm{Im}\langle T(\tilde{S}_3'\tilde{S}_3)^\dagger_{11}\rangle\}. \tag{39}$$

For brevity, a few indices are not written out in the above equations, e.g., $\theta\equiv\theta_1$, $\varphi\equiv\varphi_1$, and $\langle T(\tilde{S}_3'\tilde{S}_3)^\dagger_{KQ}\rangle \equiv\langle T((L\tilde{S}')J'(L\tilde{S})J)^\dagger_{KQ}\rangle^{\mathrm{lab}}|_{L=J'=J=3}$.

Shown in Fig. 5 are the time spectra of $I(\theta=\varphi=\pi/2;t)$, $IP_1(\theta=\varphi=\pi/2;t)$, $IP_2(\theta=\varphi=\pi/2;t)$, and $IP_3(\theta=\varphi=\pi/2;t)$ computed for two cases of $\omega=0$ and 0.4335 using the state multipoles listed in Tables I–V. In the case of $\omega=0$, the pure LS coupling scheme is assumed to be valid and there is no mixing between the singlet and triplet states. Consequently, only the $^1F_3$

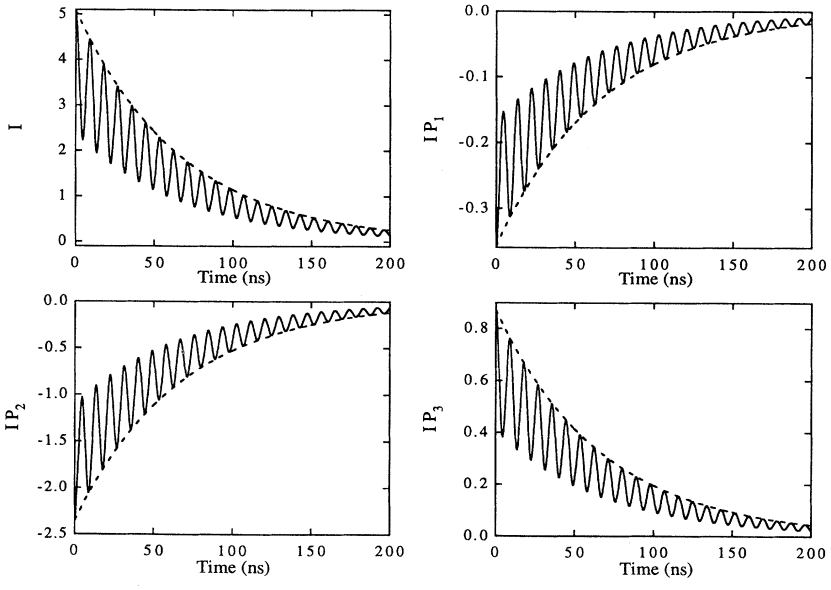

FIG. 5. Time spectra of $I(\theta=\varphi=\pi/2;t)$, $IP_1(\theta=\varphi=\pi/2;t)$, $IP_2(\theta=\varphi=\pi/2;t)$, and $IP_3(\theta=\varphi=\pi/2;t)$ of the first photon in arbitrary units. The electron incident, energy is 100 eV and the scattering angle (θ_e) is 10°. Dashed lines, $\omega=0$; solid lines, $\omega=0.4335$.

state decays to the $3\,^1D$ state and the time spectra are simple exponential curves. However, in the case of $\omega=0.4335$, both the $^1F_3$ and $^3F_3$ states can decay to the $3\,^1D$ state because both of them have mixed singlet and triplet character. The energy difference between these two states is 704 MHz, which results in time modulations in their decay curves.

Finally, we calculate the integrated polarization for the $1s4f\rightarrow 3\,^1D$ transition. In the classic paper of Percival and Seaton [30], a list of formulas was given for the integrated polarization of the photons emitted from transitions between the lowest few angular-momentum states of helium, which are well LS coupled. Since we have already derived the formulas for the total intensity and the Stokes parameters, the integrated polarization for the $1s4f\rightarrow 3\,^1D$ transition can be obtained readily by integrating Eqs. (36) and (37) over time t and photon angle φ_γ. Note that the contribution from the off-diagonal elements ($\tilde{S}'\neq\tilde{S}$). By ignoring the off-diagonal terms, which is thousands of times less than the diagonal ones in this case, we obtain

$$P_1^{\rm int}(\theta_\gamma=90^\circ)=\int_0^{2\pi} IP_1(\theta_\gamma=90^\circ,\varphi_\gamma)d\varphi_\gamma \Big/ \int_0^{2\pi} I(\theta_\gamma=90^\circ,\varphi_\gamma)d\varphi_\gamma$$

$$=\frac{3(4\bar{Q}_0+3\bar{Q}_1+3\bar{Q}_{-1}-5\bar{Q}_3-5\bar{Q}_{-3})}{24\bar{Q}_0+23\bar{Q}_1+23\bar{Q}_{-1}+20\bar{Q}_2+20\bar{Q}_{-2}+15\bar{Q}_3+15\bar{Q}_{-3}}\ , \tag{40}$$

where

$$\bar{Q}_{m_J}=\int_0^{\pi}\{|f((L=3,\tilde{S}=0)J=3,m_J)|^2 + \omega^2|f((L=3,\tilde{S}=1)J=3,m_J)|^2\}d\theta_e \tag{41}$$

and $f((L\tilde{S})Jm_J)$ are the excitation amplitudes of the mixed $|(L\tilde{S})Jm_J\rangle$ state as defined by Eqs. (9)–(11). A similar integration gives $P_2^{\rm int}=P_3^{\rm int}=0$.

B. Explicit formulas for the cascade $1s4f\rightarrow 3\,^1D\rightarrow 2\,^1P$ transitions

As illustrated in the preceding subsection, measurements of the first photon emitted from the $1s4f\rightarrow 3\,^1D$ transition would provide coherence information between the $|4\,^1F_{3m_J}\rangle$ and $|4\,^3F_{3m_J}\rangle$ states. Unfortunately, the present experimental technology does not allow a direct analysis of this photon due to the inefficiency of photon detectors in the infrared region. The same applies to the photon emitted from the $1s4f\rightarrow 3\,^3D$ transition.

An alternative choice is to analyze the cascading photon emitted from the subsequent $3\,^1D\rightarrow 2\,^1P$ transition, which has a wavelength in the visible region where efficient photon detectors exist. The expressions for describing the angular distribution and polarization of this photon can be derived in the following way. Substituting Eqs. (27), (28), and (30) into Eq. (29), one obtains an explicit expression for the density matrix describing the two photons (γ_1,γ_2) emitted from the cascading transitions $1s4f\rightarrow 3\,^1D\rightarrow 2\,^1P$,

$$\begin{aligned}
&\rho(\lambda_1'\lambda_1\vec{n}_1;t_1,\lambda_2'\lambda_2\vec{n}_2;t_2)\\
&=C_2\sum_{\substack{K_2,Q_2,q_2,K_3,Q_3,q_3,b\\ J_3'=J_3=3;\tilde{S}_3,\tilde{S}_3'}}(-1)^{\lambda_2+K_3+q_2}\hat{K}_3(\hat{K}_2\hat{b})^2\omega^0_{\tilde{S}_3'J_3'}\omega^0_{\tilde{S}_3J_3}e^{-\gamma_3 t_1-\gamma_2(t_2-t_1)}\cos[(E_{\tilde{S}_3}-E_{\tilde{S}_3})t_1/\hbar]\\
&\quad\times\begin{pmatrix}1&1&K_2\\-\lambda_2'&\lambda_2&(\lambda_2'-\lambda_2)\end{pmatrix}\begin{Bmatrix}1&1&K_2\\J_2&J_2'&J_1\end{Bmatrix}\begin{pmatrix}K_3&b&K_2\\q_3&(\lambda_1'-\lambda_1)&-q_2\end{pmatrix}\\
&\quad\times\begin{pmatrix}b&1&1\\(\lambda_1-\lambda_1')&\lambda_1'&-\lambda_1\end{pmatrix}\begin{pmatrix}K_3&b&K_2\\J_3&1&J_2\\J_3'&1&J_2'\end{pmatrix}\langle T((L_3\tilde{S}_3')J_3'(L_3\tilde{S}_3)J_3)^\dagger_{K_3Q_3}\rangle^{\rm lab}\\
&\quad\times D(0\theta_2\varphi_2)^{K_2}_{\lambda_2'-\lambda_2,Q_2}D(0\theta_1\varphi_1)^{K_3}_{q_3,Q_3}D^*(0\theta_1\varphi_1)^{K_2}_{q_2,Q_2}\ ,
\end{aligned}\tag{42}$$

where C_2 is similar to C_1 of Eq. (35) and contains all the terms that can be factored out of the summation.

Because the first photon γ_1 is not measured, we integrated the above expression over the angles of (θ_1,φ_1) and over the time t_1 $(0<t_1<t_2)$. This gives the reduced photon density matrix for coincidence measurement of (e,γ_2). The orthogonality relation of the rotation matrix

$$\int_0^{2\pi}\int_0^{\pi}D(0\theta_1\varphi_1)^{K_3}_{q_3,Q_3}D^*(0\theta_1\varphi_1)^{K_2}_{q_2,Q_2}\sin\theta\,d\theta\,d\varphi = \frac{8\pi^2}{2K_3+1}\delta_{K_2K_3}\delta_{q_2q_3}\delta_{Q_2Q_3} \tag{43}$$

was used to simplify Eq. (42) before further calculations.

The total intensity and the Stokes parameters for the second photon γ_2 are

$$I(\theta\varphi)=\sum_{\lambda_2'=\lambda_2=\pm1,\lambda_1'=\lambda_1=\pm1}\rho(\lambda_1'\lambda_1\vec{n}_1,\lambda_2'\lambda_2\vec{n}_2)\ , \tag{44}$$

$$IP_1(\theta\varphi)=-\sum_{\lambda_1'=\lambda_1=\pm1}[\rho(\lambda_2'=1,\lambda_2=-1)+\rho(\lambda_2'=-1,\lambda_2=1)]\ , \tag{45}$$

$$IP_2(\theta\varphi)=-i\sum_{\lambda_1'=\lambda_1=\pm1}[\rho(\lambda_2'=1,\lambda_2=-1)-\rho(\lambda_2'=-1,\lambda_2=1)]\ , \tag{46}$$

$$IP_3(\theta\varphi)=-\sum_{\lambda_1'=\lambda_1=\pm1}[\rho(\lambda_2'=1,\lambda_2=1)-\rho(\lambda_2'=-1,\lambda_2=-1)]\ . \tag{47}$$

Evaluation of these expressions showed that they are identical to Eqs. (36)–(39) except that C_1 is replaced by C_2, $\theta\equiv\theta_2$, $\varphi\equiv\varphi_2$, and the time-dependent part is now

$$\frac{e^{(\gamma_2-\gamma_3)t_2}[\Delta E\sin(\Delta E\,t_2)+(\gamma_2-\gamma_3)\cos(\Delta E\,t_2)]-(\gamma_2-\gamma_3)}{e^{\gamma_2 t_2}[(\gamma_2-\gamma_3)^2+\Delta E^2]}\ , \tag{48}$$

where $\Delta E=E_{\tilde{S}_3'}-E_{\tilde{S}_3}$. This suggests that the angular distribution and polarization correlations of the second photon provide essentially the same information as the first photon. Shown in Fig. 6 are the time spectra of $I(\theta_2=\varphi_2=\pi/2;t_2)$, $IP_1(\theta_2=\varphi_2=\pi/2;t_2)$, $IP_2(\theta_2=\varphi_2=\pi/2;t_2)$, and $IP_3(\theta_2=\varphi_2=\pi/2;t_2)$ of the second photon for $\omega=0$ and 0.4335. The time variations in the solid curves ($\omega=0.4335$) are clearly visible, although they are somewhat smeared by the integration.

C. Explicit formulas for the complete cascade $1s4f\rightarrow3\,^1D\rightarrow2\,^1P\rightarrow1\,^1S$ transitions

Substituting Eqs. (23), (24), (27), (28), (31), (32), and (34) into Eq. (33), we have the complete density matrix for for describing all three cascading photons,

$$\begin{aligned}&\rho(\lambda_1'\lambda_1\vec{n}_1;t_1,\lambda_2'\lambda_2\vec{n}_2;t_2,\lambda_3'\lambda_3\vec{n}_3;t_3)\\&=C_3\sum_{\substack{K_1,Q_1,K_2,q_2',Q_2,q_1\\K_3,q_3,Q_3,q_2,b,b'\\J_3'=J_3=3;\tilde{S}_3,\tilde{S}_3'}}(-1)^{\lambda_3+K_2+q_1+K_3+q_2}\hat{K}_3(\hat{K}_1\hat{K}_2\hat{b}\hat{b}')^2\omega^0_{\tilde{S}_3'J_3'}\omega^0_{\tilde{S}_3J_3}e^{-\gamma_3t_1-\gamma_2(t_2-t_1)-\gamma_1(t_3-t_2)}\\&\times\cos[(E_{\tilde{S}_3'}-E_{\tilde{S}_3})t_1/\hbar]\begin{bmatrix}1&1&K_1\\-\lambda_3'&\lambda_3&(\lambda_3'-\lambda_3)\end{bmatrix}\begin{Bmatrix}1&1&K_1\\J_1&J_1'&J_0\end{Bmatrix}\\&\times\begin{bmatrix}K_2&b'&K_1\\q_2'&(\lambda_2'-\lambda_2)&-q_1\end{bmatrix}\begin{bmatrix}b'&1&1\\(\lambda_2-\lambda_2')&\lambda_2'&-\lambda_2\end{bmatrix}\begin{bmatrix}K_2&b'&K_1\\J_2&1&J_1\\J_2'&1&J_1'\end{bmatrix}\\&\times\begin{bmatrix}K_3&b&K_2\\q_3&(\lambda_1'-\lambda_1)&-q_2\end{bmatrix}\begin{bmatrix}b&1&1\\(\lambda_1-\lambda_1')&\lambda_1'&-\lambda_1\end{bmatrix}\begin{bmatrix}K_3&b&K_2\\J_3&1&J_2\\J_3'&1&J_2'\end{bmatrix}\\&\times\langle T((L_3\tilde{S}_3')J_3'(L_3\tilde{S}_3)J_3)^\dagger_{K_3Q_3}\rangle^{\rm lab}D(0\theta_3\varphi_3)^{K_1}_{\lambda_3'-\lambda_3,Q_1}D(0\theta_2\varphi_2)^{K_2}_{q_2',Q_2}\\&\times\langle T((L_3\tilde{S}_3')J_3'(L_3\tilde{S}_3)J_3)^\dagger_{K_3Q_3}\rangle^{\rm lab}D(0\theta_3\varphi_3)^{K_1}_{\lambda_3'-\lambda_3,Q_1}D(0\theta_2\varphi_2)^{K_2}_{q_2',Q_2}\end{aligned} \tag{49}$$

where C_3 is similar to C_1 and C_2 of Eqs. (35) and (42) and contains all the terms that can be factored out of the summation.

Considering the recent success of triple coincidence measurements in He $3\,^1D$ [31], similar measurements in He $1s4f$ will be feasible in the near future. In He $3\,^1D$, one measures the coincidence rates between the scattered electron with energy loss of $\sim$23.1 eV and the two photons with wavelength of 668 nm (visible) and 58 nm (uv). In He $1s4f$, the scattered electron with energy loss of $\sim$23.8 eV is measured in coincidence with the second and third cascading photons, which have the same wavelengths of 668 and 58 nm, respectively. Such measurements will provide information about the $1s4f$ state multipoles up to rank 4.

For this reason, we derived the corresponding coin-

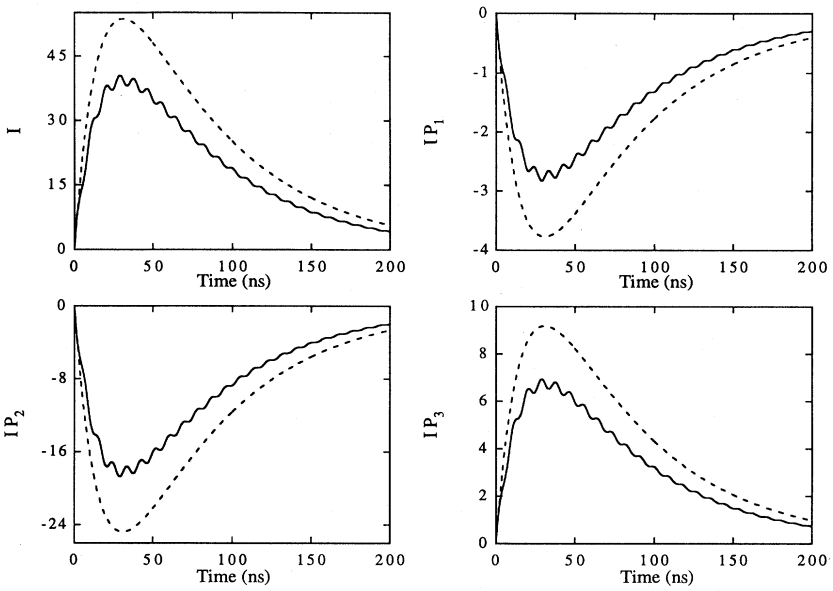

FIG. 6. Same as Fig. 5 except for the second photon (see the text).

cidence intensities and the Stokes parameters for all possible arrangements of the two photon detectors for the $1s4f$ state using Eq. (49). Again, since the first photon γ_1 is not measured, Eq. (43) was applied to simplify the three-photon density matrix. The explicit expressions obtained are too long to be listed here and readers can write to the authors (electronic address: wang@earwax.pd.uwa.edu.au) for the detailed information if required.

For illustration, we present our results for two special experimental arrangements. In the first case, both photon detectors are perpendicular to the incident electron beam with the uv detector perpendicular to the scattering plane and the visible detector in the plane, i.e., $\theta_2=\pi/2$, $\varphi_2=0$, $\theta_3=\pi/2$, and $\varphi_3=\pi/2$. The coincidence intensity and the Stokes parameters are found to be

$$I=C_3\sum_{\tilde{S}_3',\tilde{S}_3}\omega^0_{\tilde{S}_3'J_3'}\omega^0_{\tilde{S}_3J_3}e^{-\gamma_3 t_1-\gamma_2(t_2-t_1)-\gamma_1(t_3-t_2)}\cos[(E_{\tilde{S}_3'}-E_{\tilde{S}_3})t_1/\hbar]$$
$$\times\tfrac{1}{42}[-182\sqrt{7}\langle T(\tilde{s}_3'\tilde{s}_3)^\dagger_{00}\rangle+32\sqrt{21}\langle T(\tilde{s}_3';\tilde{s}_3)^\dagger_{20}\rangle-\sqrt{154}\langle T(\tilde{s}_3'\tilde{s}_3)^\dagger_{40}\rangle+14\sqrt{55}\langle T(\tilde{s}_3'\tilde{s}_3)^\dagger_{44}\rangle], \quad (50)$$

$$IP_1=C_3\sum_{\tilde{S}_3'\tilde{S}_3}\omega^0_{\tilde{S}_3'J_3'}\omega^0_{\tilde{S}_3J_3}e^{-\gamma_3 t_1-\gamma_2(t_2-t_1)-\gamma_1(t_3-t_2)}\cos[(E_{\tilde{S}_3'}-E_{\tilde{S}_3})t_1/\hbar]$$
$$\times\tfrac{1}{42}[-14\sqrt{7}\langle T(\tilde{S}_3'\tilde{S}_3)^\dagger_{00}\rangle+56\sqrt{21}\langle T(\tilde{S}_3'\tilde{S}_3)^\dagger_{20}\rangle-72\sqrt{14}\langle T(\tilde{S}_3'\tilde{S}_3)^\dagger_{22}\rangle$$
$$-7\sqrt{154}\langle T(\tilde{S}_3'\tilde{S}_3)^\dagger_{40}\rangle+8\sqrt{385}\langle T(\tilde{S}_3'\tilde{S}_3)^\dagger_{42}\rangle-14\sqrt{55}\langle T(\tilde{S}_3'\tilde{S}_3)^\dagger_{44}\rangle], \quad (51)$$

$$IP_2=C_3\sum_{\tilde{S}_3',\tilde{S}_3}\omega^0_{\tilde{S}_3',J_3'}\omega^0_{\tilde{S}_3J_3}e^{-\gamma_3 t_1-\gamma_2(t_2-t_1)-\gamma_1(t_3-t_2)}\cos[(E_{\tilde{S}_3'}-E_{\tilde{S}_3})t_1/\hbar]$$
$$\times\frac{\sqrt{2}}{21}[-60\sqrt{7}\langle T(\tilde{S}_3'\tilde{S}_3)^\dagger_{21}\rangle+3\sqrt{385}\langle T(\tilde{S}_3'\tilde{S}_3)^\dagger_{41}\rangle-7\sqrt{55}\langle T(\tilde{S}_3'\tilde{S}_3)^\dagger_{43}\rangle], \quad (52)$$

$$IP_3=C_3\sum_{\tilde{S}_3',\tilde{S}_3}\omega^0_{\tilde{S}_3'J_3'}\omega^0_{\tilde{S}_3J_3}e^{-\gamma_3 t_1-\gamma_2(t_2-t_1)-\gamma_1(t_3-t_2)}\cos[(E_{\tilde{S}_3'}-E_{\tilde{S}_3})t_1/\hbar]$$
$$\times\sqrt{2}[4\sqrt{7}\,\mathrm{Im}\langle T(\tilde{S}_3'\tilde{S}_3)^\dagger_{11}\rangle-\mathrm{Im}\langle T(\tilde{S}_3'\tilde{S}_3)^\dagger_{31}\rangle+\sqrt{15}\,\mathrm{Im}\langle T(\tilde{S}_3'\tilde{S}_3)^\dagger_{33}\rangle]. \quad (53)$$

In the second case, we chose $\theta_2=\pi/2$, $\varphi_2=0$, $\theta_3=\pi/3$, and $\varphi_3=\pi/2$ and the coincidence intensity and the Stokes parameters are

$$I=C_3\sum_{\tilde{S}_3',\tilde{S}_3}\omega^0_{\tilde{S}_3'J_3'}\omega^0_{\tilde{S}_3J_3}e^{-\gamma_3 t_1-\gamma_2(t_2-t_1)-\gamma_1(t_3-t_2)}\cos[(E_{\tilde{S}_3'}-E_{\tilde{S}_3})t_1/\hbar]$$
$$\times\tfrac{1}{168}[-728\sqrt{7}\langle T(\tilde{S}_3'\tilde{S}_3)^\dagger_{00}\rangle+80\sqrt{21}\langle T(\tilde{S}_3'\tilde{S}_3)^\dagger_{20}\rangle+\sqrt{154}\langle T(\tilde{S}_3'\tilde{S}_3)^\dagger_{40}\rangle$$
$$-48\sqrt{14}\langle T(\tilde{S}_3'\tilde{S}_3)^\dagger_{22}\rangle-4\sqrt{385}\langle T(\tilde{S}_3'\tilde{S}_3)^\dagger_{42}\rangle+42\sqrt{55}\langle T(\tilde{S}_3'\tilde{S}_3)^\dagger_{44}\rangle], \quad (54)$$

$$IP_1 = C_3 \sum_{\tilde{S}'_3,\tilde{S}_3} \omega^0_{\tilde{S}'_3 J'_3} \omega^0_{\tilde{S}_3 J_3} e^{-\gamma_3 t_1 - \gamma_2 (t_2 - t_1) - \gamma_1 (t_3 - t_2)} \cos[(E_{\tilde{S}'_3} - E_{\tilde{S}_3}) t_1 / \hbar]$$
$$\times \tfrac{1}{168} [-56\sqrt{7} \langle T(\tilde{S}'_3 \tilde{S}_3)^\dagger_{00} \rangle + 176\sqrt{21} \langle T(\tilde{S}'_3 \tilde{S}_3)^\dagger_{20} \rangle - 23\sqrt{154} \langle T(\tilde{S}'_3 \tilde{S}_3)^\dagger_{40} \rangle$$
$$- 336\sqrt{14} \langle T(\tilde{S}'_3 \tilde{S}_3)^\dagger_{22} \rangle + 28\sqrt{385} \langle T(\tilde{S}'_3 \tilde{S}_3)^\dagger_{42} \rangle - 70\sqrt{55} \langle T(\tilde{S}'_3 \tilde{S}_3)^\dagger_{44} \rangle] , \quad (55)$$

$$IP_2 = C_3 \sum_{\tilde{S}'_3,\tilde{S}_3} \omega^0_{\tilde{S}'_3 J'_3} \omega^0_{\tilde{S}_3 J_3} e^{-\gamma_3 t_1 - \gamma_2 (t_2 - t_1) - \gamma_1 (t_3 - t_2)} \cos[(E_{\tilde{S}'_3} - E_{\tilde{S}_3}) t_1 / \hbar]$$
$$\times \tfrac{1}{42} [-60\sqrt{42} \langle T(\tilde{S}'_3 \tilde{S}_3)^\dagger_{21} \rangle + 3\sqrt{2310} \langle T(\tilde{S}'_3 \tilde{S}_3)^\dagger_{41} \rangle - 7\sqrt{330} \langle T(\tilde{S}'_3 \tilde{S}_3)^\dagger_{43} \rangle] , \quad (56)$$

$$IP_3 = C_3 \sum_{\tilde{S}'_3,\tilde{S}_3} \omega^0_{\tilde{S}'_3 J'_3} \omega^0_{\tilde{S}_3 J_3} e^{-\gamma_3 t_1 - \gamma_2 (t_2 - t_1) - \gamma_1 (t_3 - t_2)} \cos[(E_{\tilde{S}'_3} - E_{\tilde{S}_3}) t_1 / \hbar]$$
$$\times \tfrac{1}{2} [4\sqrt{42} \, \mathrm{Im} \langle T(\tilde{S}'_3 \tilde{S}_3)^\dagger_{11} \rangle - \sqrt{6} \, \mathrm{Im} \langle T(\tilde{S}'_3 \tilde{S}_3)^\dagger_{31} \rangle + 3\sqrt{10} \, \mathrm{Im} \langle T(\tilde{S}'_3 \tilde{S}_3)^\dagger_{33} \rangle] . \quad (57)$$

It can be seen the measurements at different angles reveal different components of the $1s4f$ state multipoles. Accordingly, we know from the full formulas the best positioning of the photon detectors for measurement of each state multipole. This provides guidance for optimum experimental design to ensure the most efficient and revealing measurements.

IV. CONCLUSION

In this paper, we have presented a general framework for treating the time evolution and the cascading decay process of helium $1s4f$ state, which has mixed singlet and triplet characters and its sublevels are coherently excited by electron impact. Explicit formulas for the coincidence intensity and Stokes parameters associated with measurements of (e,γ_1), (e,γ_2), and (e,γ_2,γ_3) are derived. The excitation amplitudes are calculated using the first-order DWBA method for incident energy of 100 eV. It is found that the intensity and polarization of the first photon from the $1s4f \rightarrow 3\,^1D$ transition are time modulated due to the singlet and triplet mixing in the $1s4f$ state. Quantum beats also appear in the time spectra of the cascade photon from the subsequent $3\,^1D \rightarrow 2\,^1P$ transition.

The transitions considered in this work are $1s4f \rightarrow 3\,^1D \rightarrow 2\,^1P \rightarrow 1\,^1S$, which reveal coherent information between the $|4\,^1F_3\rangle$ and $|4\,^3F_3\rangle$ levels. For coherent information between all four levels of the $1s4f$ state, i.e., $|4\,^1F_3\rangle$ and $|4\,^3F_{2,3,4}\rangle$, an analysis of the transitions $1s4f \rightarrow 3\,^3D \rightarrow 2\,^3P \rightarrow 2\,^3S$ is required, which will be the topic of a separate paper.

ACKNOWLEDGMENT

This work was supported by the Australian Research Council.

APPENDIX

The details of derivation of the trace expressions arising from the density-matrix computation are given for completeness in this appendix.

1. Derivation of Eq. (24)

The time evolution coefficient is

$$G((LS')J'(LS)J;t)$$
$$= \mathrm{Tr}\{ U(t) T((LS')J'(LS)J)_{KQ} U(t)^\dagger T((LS')J'(LS)J)^\dagger_{kq} \}$$
$$= \sum_{m,m',J'',m'',J''',m'''} \langle (LS)Jm | U(t) | (LS'')J''m'' \rangle \langle (LS'')J''m'' | T((LS')J'(LS)J)_{KQ} | (LS')J'm' \rangle$$
$$\times \langle (LS')J'm' | U(t)^\dagger | (LS''')J'''m''' \rangle \langle (LS''')J'''m''' | T((LS')J'(LS)J)^\dagger_{kq} | (LS)Jm \rangle ,$$

where the various terms are

$$\langle (LS)Jm | U(t) | (LS'')J''m'' \rangle = e^{-\gamma t/2 - iE_{(LS)J} t/\hbar} \delta_{JJ''} \delta_{mm''} ,$$
$$\langle (LS')J'm' | U(t)^\dagger | (LS''')J'''m''' \rangle = e^{-\gamma t/2 + iE_{(LS')J'} t/\hbar} \delta_{J'J'''} \delta_{m'm'''} ,$$
$$\langle (LS'')J''m'' | T((LS')J'(LS)J)_{KQ} | (LS')J'm' \rangle = (-1)^{J-m} \begin{pmatrix} J & J' & K \\ m & -m' & -Q \end{pmatrix} \hat{K} ,$$
$$\langle (LS''')J'''m''' | T((LS')J'(LS)J)^\dagger_{kq} | (LS)Jm \rangle = (-1)^{J-m} \begin{pmatrix} J & J' & k \\ m & -m' & -q \end{pmatrix} \hat{k} .$$

Note that

$$\sum_{m,m'} \begin{bmatrix} J & J' & K \\ m & -m' & -Q \end{bmatrix} \begin{bmatrix} J & J' & k \\ m & -m' & -q \end{bmatrix} = \frac{1}{2K+1} \delta_{Kk} \delta_{Qq}$$

and the final result is thus

$$G((LS')J'(LS)J;t) = e^{-\gamma t - i[E_{(LS)J} - E_{(LS')J'}]t/\hbar} \delta_{Kk} \delta_{Qq} \ .$$

2. Derivation of Eq. (26)

The trace is calculated in the complete basis of the lower states

$$\begin{aligned}
&\mathrm{Tr}\{r_{-\lambda_1'} T((L_3\tilde{S}_3')J_3'(L_3\tilde{S}_3)J_3)_{K_3q_3} r^\dagger_{-\lambda_1}\}^{\vec{n}_1} \\
&= \sum_{J_2,m_2,m_3,m_3'} \langle (L_2S_2)J_2m_2 | r_{-\lambda_1'} | (L_3'\tilde{S}_3')J_3'm_3' \rangle \\
&\qquad \times \langle (L_3'\tilde{S}_3')J_3'm_3' | T((L_3\tilde{S}_3')J_3'(L_3\tilde{S}_3)J_3)^{\vec{n}_1}_{K_3q_3} | (L_3\tilde{S}_3)J_3m_3 \rangle \langle (L_3\tilde{S}_3)J_3m_3 | r^\dagger_{-\lambda_1} | (L_2S_2)J_2m_2 \rangle \\
&= \sum_{J_2,m_2,m_3,m_3'} (-1)^{J_2-m_2} \begin{bmatrix} J_2 & 1 & J_3' \\ -m_2 & -\lambda_1' & m_3' \end{bmatrix} \langle (L_2S_2)J_2 \| \vec{r} \| (L_3\tilde{S}_3')J_3' \rangle \\
&\qquad \times (-1)^{J_3'-m_3'} \hat{K}_3 \begin{bmatrix} J_3' & K_3 & J_3 \\ -m_3' & q_3 & m_3 \end{bmatrix} (-1)^{J_2-m_2} \begin{bmatrix} J_2 & 1 & J_3 \\ -m_2 & -\lambda_1 & m_3 \end{bmatrix} \langle (L_2S_2)J_2 \| \vec{r} \| (L_3\tilde{S}_3)J_3 \rangle^* \\
&= \sum_{J_2} (-1)^{J_2+J_3'+\lambda_1} \hat{K}_3 \begin{bmatrix} 1 & 1 & K_3 \\ -\lambda_1' & \lambda_1 & q_3 \end{bmatrix} \begin{Bmatrix} 1 & 1 & K_3 \\ J_3 & J_3' & J_2 \end{Bmatrix} \langle (L_2S_2)J_2 \| \vec{r} \| (L_3\tilde{S}_3')J_3' \rangle \langle (L_2S_2)J_2 \| \vec{r} \| (L_3\tilde{S}_3)J_3 \rangle^* \ ,
\end{aligned}$$

where

$$\begin{aligned}
\langle (L_2S_2)J_2 \| \vec{r} \| (L_3\tilde{S}_3')J_3' \rangle &= \langle (L_2S_2)J_2 \| \vec{r} \| \omega^0_{\tilde{S}_3'J_3'}(L_30)J_3' + \omega^1_{\tilde{S}_3'J_3'}(L_31)J_3' \rangle \\
&= (-1)^{L_2+J_3'} \hat{J}_2 \hat{J}_3' \langle L_2 \| \vec{r} \| L_3 \rangle \left[\omega^1_{\tilde{S}_3'J_3'} \begin{Bmatrix} L_2 & J_2 & 1 \\ J_3' & L_3 & 1 \end{Bmatrix} \delta_{S_21} - \omega^0_{\tilde{S}_3'J_3'} \begin{Bmatrix} L_2 & J_2 & 0 \\ J_3' & L_3 & 1 \end{Bmatrix} \delta_{S_20} \right] , \\
\langle (L_2S_2)J_2 \| \vec{r} \| (L_3\tilde{S}_3)J_3 \rangle^* &= \langle (L_2S_2)J_2 \| \vec{r} \| \omega^0_{\tilde{S}_3J_3}(L_30)J_3 + \omega^1_{\tilde{S}_3J_3}(L_31)J_3 \rangle^* \\
&= (-1)^{L_2+J_3} \hat{J}_2 \hat{J}_3 \langle L_2 \| \vec{r} \| L_3 \rangle^* \left[\omega^1_{\tilde{S}_3J_3} \begin{Bmatrix} L_2 & J_2 & 1 \\ J_3 & L_3 & 1 \end{Bmatrix} \delta_{S_21} - \omega^0_{\tilde{S}_3J_3} \begin{Bmatrix} L_2 & J_2 & 0 \\ J_3 & L_3 & 1 \end{Bmatrix} \delta_{S_20} \right] ,
\end{aligned}$$

and $\omega^0_{1,2} = \omega^0_{1,4} = 0$, $\omega^1_{1,2} = \omega^1_{1,4} = 1$, $\omega^0_{0,3} = \omega^1_{1,3} = 1/\sqrt{1+\omega^2}$, and $\omega^1_{0,3} = -\omega^0_{0,3} = \omega/\sqrt{1+\omega^2}$.

3. Derivation of Eq. (28)

This trace is calculated similarly to that above:

$$\begin{aligned}
&\mathrm{Tr}\{r_{-\lambda_1'} (T((L_3\tilde{S}_3)J_3'(L_3\tilde{S}_3)J_3)_{K_3q_3} r^\dagger_{-\lambda_1} T((L_2S_2)J_2'J_2)^\dagger_{K_2q_2}\}^{\vec{n}} \\
&= \sum_{m_2,m_2',m_3,m_3'} \langle (L_2S_2)J_2m_2 | r_{-\lambda_1'} | (L_3\tilde{S}_3)J_3m_3 \rangle \langle (L_3\tilde{S}_3)J_3m_3 | T((L_3\tilde{S}_3')J_3'(L_3\tilde{S}_3)J_3)_{K_3q_3} | (L_3'\tilde{S}_3')J_3'm_3' \rangle \\
&\qquad \times \langle (L_3'\tilde{S}_3')J_3'm_3' | r^\dagger_{-\lambda_1} | (L_2S_2)J_2'm_2' \rangle \langle (L_2S_2)J_2'm_2' | T(J_2'J_2)^\dagger_{K_2q_2} | (L_2S_2)J_2m_2 \rangle \\
&= \sum_{m_2,m_2',m_3,m_3'} (-1)^{J_2-m_2} \begin{bmatrix} J_2 & 1 & J_3 \\ -m_2 & -\lambda_1' & m_3 \end{bmatrix} \langle (L_2S_2)J_2 \| \vec{r} \| (L_3\tilde{S}_3)J_3 \rangle \\
&\qquad \times (-1)^{J_3-m_3} \hat{K}_3 \begin{bmatrix} J_3 & K_3 & J_3' \\ -m_3 & q_3 & m_3' \end{bmatrix} (-1)^{J_2'-m_2'} \begin{bmatrix} J_2' & 1 & J_3' \\ -m_2' & -\lambda_1 & m_3' \end{bmatrix} \\
&\qquad \times \langle (L_2S_2)J_2' \| \vec{r} \| (L_3\tilde{S}_3')J_3' \rangle^* (-1)^{J_2-m_2} \hat{K}_2 \begin{bmatrix} J_2 & K_2 & J_2' \\ -m_2 & q_2 & m_2' \end{bmatrix}
\end{aligned}$$

$$=\hat{K}_2\hat{K}_3\langle(L_2S_2)J_2\|\vec{r}\|(L_3\tilde{S}_3)J_3\rangle\langle(L_2S_2)J_2'\|\vec{r}\|(L_3\tilde{S}_3')J_3'\rangle^*$$

$$\times(-1)^{K_3+q_3}\sum_b(2b+1)\begin{bmatrix}K_3 & b & K_2\\ q_3 & (\lambda_1'-\lambda_1) & -q_2\end{bmatrix}\begin{bmatrix}b & 1 & 1\\ (\lambda_1-\lambda_1') & \lambda_1' & -\lambda_1\end{bmatrix}\begin{bmatrix}K_3 & b & K_2\\ J_3 & 1 & J_2\\ J_3' & 1 & J_2'\end{bmatrix}.$$

Note that the contraction rule

$$\sum_{\phi,\nu,\delta,\rho}\begin{bmatrix}c & f & i\\ \gamma & \phi & \nu\end{bmatrix}\begin{bmatrix}a & d & g\\ \alpha & \delta & \rho\end{bmatrix}\begin{bmatrix}d & e & f\\ \delta & \varepsilon & \phi\end{bmatrix}\begin{bmatrix}g & h & i\\ \rho & \eta & \nu\end{bmatrix}=\sum_b(2b+1)\begin{bmatrix}a & b & c\\ \alpha & \beta & \gamma\end{bmatrix}\begin{bmatrix}b & e & h\\ \beta & \varepsilon & \eta\end{bmatrix}\begin{bmatrix}a & b & c\\ d & e & f\\ g & h & i\end{bmatrix}$$

has been used.

[1] I. Bray and A. T. Stelbovics, Phys. Rev. A **48**, 4787 (1993).
[2] D. H. Madison, K. Bartschat, and R. P. McEachran, J. Phys. B **25**, 5199 (1992).
[3] M. P. Scott and P. G. Burke, J. Phys. B **26**, L191 (1993).
[4] U. Fano and J. Macek, Rev. Mod. Phys. **45**, 553 (1973).
[5] K. Blum, *Density Matrix Theory and Applications* (Plenum, New York, 1981).
[6] H. B. van Linden van den Heuvell, G. Nienhuis, J. van Eck, and H. G. M. Heideman, J. Phys. B **14**, 2667 (1981).
[7] J. Burgdörder, Phys. Rev. A **24**, 1756 (1981).
[8] E. L. Heck and J. Gauntlett, J. Phys. B **19**, 3633 (1986).
[9] J. B. Wang, A. T. Stelbovics, and J. F. Williams, Z. Phys. D **30**, 119 (1994).
[10] S. Chwirot and J. Slevin, J. Phys. B **20**, 3885 (1987).
[11] A. T. Stelbovics, M. Kumar, and J. F. Williams, J. Phys. B **26**, L237 (1993).
[12] S. Chwirot, S. Legowski, J. Slevin, and J. Zaremba, J. Phys. B **22**, 1411 (1989).
[13] N. Andersen, J. W. Gallagher, and I. V. Hertel, Phys. Rep. **165**, 1 (1988).
[14] J. A. Slevin and S. Chwirot, Comments At. Mol. Phys. **26**, 11 (1991).
[15] A. G. Mikosza, R. Hippler, J. B. Wang, and J. F. Williams, Phys. Rev. Lett. **71**, 235 (1993).
[16] G. von Oppen, Phys. Scr. **T26**, 34 (1989).
[17] D. Kaiser, Y. Q. Liu, and G. von Oppen, J. Phys. B **26**, 363 (1993).
[18] R. M. Paris and R. W. Mires, Phys. Rev. A **4**, 2145 (1971).
[19] D. R. Cok and S. R. Lundeen, Phys. Rev. A **19**, 1830 (1979).
[20] D. R. Cok and S. R. Lundeen, Phys. Rev. A **23**, 2488 (1981).
[21] J. S. Sims and W. C. Martins, Phys. Rev. A **37**, 2259 (1988).
[22] Y. Q. Liu, W. Simons, F. Walachowicz, and G. von Oppen, J. Phys. B **26**, 381 (1993).
[23] G. A. Khayrallah and S. J. Smith, Phys. Rev. A **18**, 559 (1978).
[24] A. F. J. van Raan and H. G. M. Heideman, J. Phys. B **7**, L216 (1974).
[25] F. Nienhuis, in *Coherence and Correlation in Atomic Collisions,* edited by H. Kleinpoppen and J. F. Williams (Plenum, New York, 1980), p. 121.
[26] K. Bartschat and D. H. Madison, J. Phys. B **20**, 5839 (1987).
[27] K. Bartschat and D. H. Madison, J. Phys. B **21**, 153 (1988).
[28] C. Froese Fischer, Comput. Phys. Commun. **4**, 107 (1972).
[29] J. B. Wang and J. F. Williams, Comput. Phys. Commun. **75**, 275 (1993).
[30] I. C. Percival and M. J. Seaton, Philos. Trans. R. Soc. London Ser. A **251**, 113 (1958).
[31] A. G. Mikosza, J. F. Williams, J. H. Flexman, R. Hippler, J. B. Wang, and P. A. Smith (unpublished).